BIOCHEMISTRY
including biophysical chemistry & molecular biology

Article

pubs.acs.org/biochemistry

Probing the Structural and Energetic Basis of Kinesin−Microtubule Binding Using Computational Alanine-Scanning Mutagenesis

Minghui Li and Wenjun Zheng*

Physics Department, University at Buffalo, Buffalo, New York 14260, United States

Supporting Information

ABSTRACT: Kinesin−microtubule (MT) binding plays a critical role in facilitating and regulating the motor function of kinesins. To obtain a detailed structural and energetic picture of kinesin−MT binding, we performed large-scale computational alanine-scanning mutagenesis based on long-time molecular dynamics (MD) simulations of the kinesin−MT complex in both ADP and ATP states. First, we built three all-atom kinesin−MT models: human conventional kinesin bound to ADP and mouse KIF1A bound to ADP and ATP. Then, we performed 30 ns MD simulations followed by kinesin−MT binding free energy calculations for both the wild type and mutants obtained after substitution of each charged residue of kinesin with alanine. We found that the kinesin−MT binding free energy is dominated by van der Waals interactions and further enhanced by electrostatic interactions. The calculated mutational changes in kinesin−MT binding free energy are in excellent agreement with results of an experimental alanine-scanning study with a root-mean-square error of ∼0.32 kcal/mol [Woehlke, G., et al. (1997) *Cell 90*, 207−216]. We identified a set of important charged residues involved in the tuning of kinesin−MT binding, which are clustered on several secondary structural elements of kinesin (including well-studied loops L7, L8, L11, and L12, helices α4, α5, and α6, and less-explored loop L2). In particular, we found several key residues that make different contributions to kinesin−MT binding in ADP and ATP states. The mutations of these residues are predicted to fine-tune the motility of kinesin by modulating the conformational transition between the ADP state and the ATP state of kinesin.

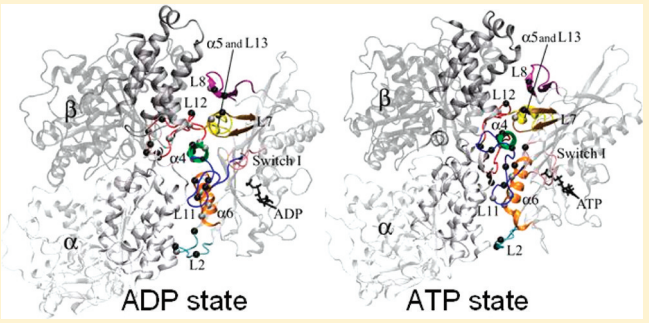

Kinesins, a superfamily of microtubule-based motor proteins, are involved in many important cellular functions, including cell division and the transport of organelles, vesicles, and other cellular cargo.[2,3] Kinesin converts the chemical energy liberated from ATP hydrolysis to mechanical work that generates movement along the microtubule (MT) track,[2] which is composed of repeating dimeric subunits formed by an α- and β-tubulin monomer.[4] There are at least 14 classes of kinesins.[5,6] A kinesin molecule consists of a catalytic core domain that exhibits MT-stimulated ATPase activity,[7] a neck region serving as a mechanical amplifier,[8] a stalk domain for dimerization, and a tail domain for cargo binding.

The primary biochemical pathway of a monomeric kinesin in the presence of MT has been outlined by extensive kinetic studies.[9−13] Starting from a weak MT-binding ADP state, MT binding to kinesin stimulates ADP release,[14] which leads to a strong MT-binding nucleotide-free state. Then ATP binding is thought to trigger the generation of force via the docking of the neck linker along the catalytic core domain.[8,15] ATP hydrolysis and subsequent release of inorganic phosphate (P_i) return kinesin to the ADP state. The kinetic parameters of the states and transitions mentioned above vary greatly among different kinesins, which give rise to diverse motor properties. For example, although most kinesins have low MT binding affinities in the ADP state, KIF1A has enhanced affinity for MT in the ADP state,[16] which underscores its unusual ability to diffuse processively along MT as a monomer.[17]

The structural basis of kinesin kinetics remains elusive because detailed structural information is not available for all biochemical states. High-resolution crystal structures were determined only in the absence of MT for kinesins bound to various nucleotide analogues.[16,18,19] To date, a strongly bound kinesin−MT complex can be modeled only by fitting a kinesin crystal structure and an MT model[20,21] into cryo-electron microscopy (EM) maps of kinesin-decorated MT filaments.[15,18,22−26] The EM-based modeling has shed some light on the interface between kinesin and MT, where several secondary structural elements of kinesin are in the proximity of α- and β-tubulin (see Figure 1). The kinesin−MT interface is populated by many charged residues (primarily positive in kinesin and negative in MT), which suggests that electrostatics plays an important role in kinesin−MT binding. However, it remains unknown how much is contributed by electrostatic force and other forces (such as van der Waals interaction), and how much is contributed by individual residues.

Received: May 27, 2011
Revised: August 17, 2011
Published: September 12, 2011

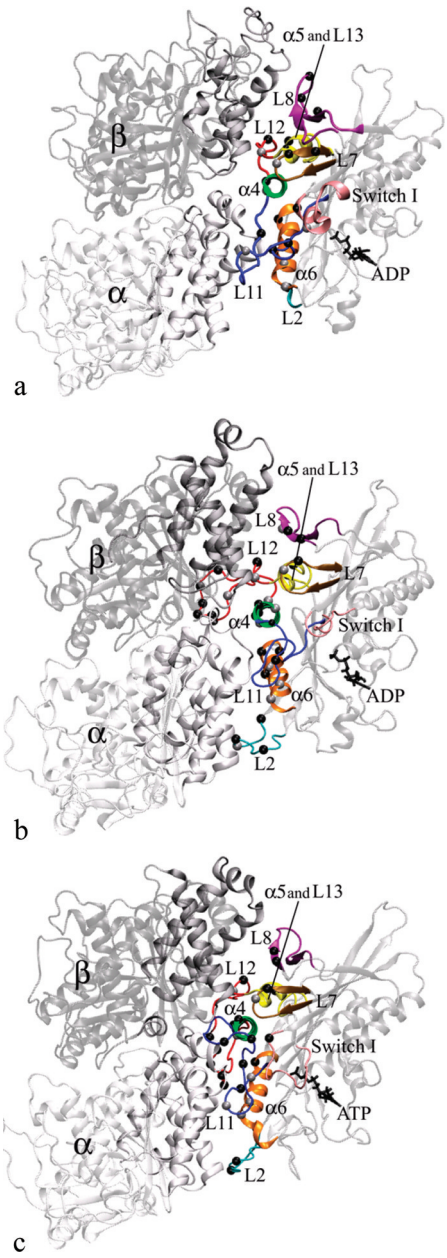

Figure 1. Average structures based on the last 10 ns of MD simulations of (a) KHC_{ADP}, (b) $KIF1A_{ADP}$, and (c) $KIF1A_{ATP}$. Kinesin, α-tubulin, and β-tubulin are colored silver, white, and gray, respectively. The key secondary structural elements of kinesin are colored as follows: loop L2 in cyan, loop L7 in ochre, loop L8 in purple, switch I in pink, loop L11 in blue, helix α4 in green, loop L12 in red, helix α5 and loop L13 in yellow, and helix α6 in orange. The charged kinesin residues predicted to be involved in kinesin–MT binding are shown as spheres (positively and negatively charged residues are colored black and silver, respectively). For details of interactions involving these residues, see Figures S1–S3 of the Supporting Information.

Computer modeling techniques, ranging from kinetic modeling[27,28] to structure-based coarse-grained modeling[29–33] and all-atom simulations,[34] have complemented experimental efforts to probe kinesin motor function. Molecular dynamics (MD) simulations[34] based on all-atom force fields[35] provide a powerful tool for investigating protein dynamics in the presence of solvents for tens of nanoseconds. Previously, several MD simulations were performed to investigate the structure and function of various kinesins in the absence of MT.[36–39] In a recent study, Aprodu el al.[40] investigated kinesin–MT binding in four nucleotide states (nucleotide-free, ATP, ADP·P_i, and ADP states) by performing 1 ns steered molecular dynamics simulations. However, detailed calculation of the kinesin–MT binding free energy remains to be done, and short MD simulations may be inadequate for probing the dynamic interactions between kinesin and MT.

To probe kinesin–MT binding at the residue level of detail, we have performed computational alanine-scanning mutagenesis to calculate the change in kinesin–MT binding free energy upon mutation of a charged kinesin residue to alanine, which is based on long-time MD simulations of the wild-type kinesin–MT complex in both ADP and ATP states. Computational alanine-scanning mutagenesis has been widely used to dissect the roles of individual residue side chains in protein–protein and protein–ligand binding.[41–51] First, we have built three kinesin–MT models: human conventional kinesin (KHC) bound to ADP[52] and mouse KIF1A bound to ADP and ATP.[53] KHC and KIF1A were chosen because of the availability of their crystal structures and biochemical data. Then we have performed 30 ns all-atom MD simulations with explicit solvents followed by computational alanine-scanning mutagenesis of all charged residues of the kinesin motor domain. We have found that the kinesin–MT binding free energy is dominated by van der Waals interactions and further enhanced by electrostatic interactions. We have identified an important set of charged residues involved in the tuning of kinesin–MT binding, which are clustered on several secondary structural elements of kinesin (see Figure 1). The calculated mutational changes in kinesin–MT binding free energy are in excellent agreement with results of a previous alanine-scanning mutagenesis study.[1] In particular, we have found several key residues contributing differently to kinesin–MT binding in the ADP and ATP states. The mutations of these residues are predicted to modulate the MT binding affinity of these two states, thereby affecting the motility properties of kinesin.

METHODS

Model Preparation. Three models of the kinesin–MT complex were obtained in previous studies by fitting a kinesin crystal structure into a cryo-EM map of kinesin-decorated MT.[52,53] The first model (named KHC_{ADP}) consists of an ADP-bound human conventional kinesin [Protein Data Bank (PDB) entry 1BG2] in a complex with α- and β-tubulin.[52] The second model (named $KIF1A_{ADP}$) consists of an ADP-bound mouse KIF1A (PDB entry 1I5S) in a complex with α- and β-tubulin.[53] The third model (named $KIF1A_{ATP}$) consists of an ATP analogue-bound mouse KIF1A (PDB entry 1VFV) in a complex with α- and β-tubulin.[53] A nucleotide (ADP or ATP) and an Mg^{2+} ion are modeled at the active site. We use the MODLOOP server[54] to model the missing residues of KHC (residues 1 and 2), KIF1A (residues 1–3, 256–260, and 290–303 of $KIF1A_{ADP}$ and residues 1, 2, 206–212, 254–268, and 289–302 of $KIF1A_{ATP}$), and MT (residues 1 and 440–451 of α-tubulin and residues 1 and 438–455 of β-tubulin). A long missing region (residues 35–60) in α-tubulin is modeled on the basis of the structure of the corresponding region in β-tubulin. The hydrogen atoms are added with VMD.[55] All models are immersed into rectangular boxes of water molecules extending up to 10 Å from the proteins in each direction by using VMD. To ensure an ionic concentration of 150 mM and zero net

charge, 70 Na^+ and 14 Cl^- ions, 69 Na^+ and 21 Cl^- ions, and 64 Na^+ and 17 Cl^- ions are added to KHC_{ADP}, $KIF1A_{ADP}$, and $KIF1A_{ATP}$, respectively, with VMD. In total, there are 107983, 117503, and 104920 atoms in KHC_{ADP}, $KIF1A_{ADP}$, and $KIF1A_{ATP}$, respectively.

MD Simulation Protocol. The three kinesin−MT systems are optimized and equilibrated using energy minimization and MD simulation. First, a 2000-step energy minimization is conducted using the steepest descent method. Then the systems are subjected to a 30 ns unconstrained MD simulation performed in the NPT ensemble. The Nosé−Hoover method[56] is used with a temperature of 300 K and a pressure of 1 atm. Periodic boundary conditions are applied to the systems. A 10 Å switching distance and a 12 Å cutoff distance are used for nonbonded interactions. The particle mesh Ewald (PME) method[57] is used to calculate long-range electrostatic interactions. The SHAKE algorithm[58] is used to constrain bond lengths of hydrogen-containing bonds, which allows a time step of 2 fs for MD simulations. The coordinates of the systems are saved every 1 ps during MD simulations for later analysis. The energy minimization and MD simulation are conducted with NAMD version 2.7b2[59] using the CHARMM27 force field[60] and TIP3P water model.[61]

Estimation of Experimental Kinesin−MT Binding Free Energy ΔG_{exp} and Its Mutational Change $\Delta\Delta G_{exp}$. In an experimental alanine-scanning mutagenesis study,[1] 36 residues of KHC were mutated to alanine and the mutants were characterized by ATPase assays that measured the apparent Michaelis−Menten constant for microtubule-dependent ATPase activation (K_{mMT}) and the maximal ATP turnover rate (k_{cat}). On the basis of kinetic analysis,[1] it was argued that $K_{mMT} \sim k_{cat}K_d(D)/k_4$, where $K_d(D)$ is the equilibrium dissociation constant for microtubules in the ADP state and k_4 represents the first-order rate constant for ADP release. Thus, using $K_{mMT} \sim 1.1$ μM, $k_{cat} \sim 27$ s^{-1},[1,1] and $k_4 \sim 300$ s^{-1},[1,10] one can estimate $\Delta G_{exp} \sim k_BT \ln(K_{mMT} \times k_4/k_{cat}) \sim -6.8$ kcal/mol. Alternatively, using the measured apparent dissociation constant of KHC construct K332 in the presence of ADP [$K_d(D) \sim 16$ μM[11]], one can estimate $\Delta G_{exp} = k_BT \ln[K_d(D)] \sim -6.6$ kcal/mol.

In ref 1, the ratios of K_{mMT} and k_{cat} between each alanine mutant and the wild type were measured [denoted as K_{mMT}' and k_{cat}', respectively (see Table 1 of ref 1)]. Thus, the mutational change in binding free energy ($\Delta\Delta G_{exp}$) for each alanine mutant can be estimated as $k_BT \ln(K_{mMT}'/k_{cat}')$.

From the measurement of apparent dissociation constants of KIF1A [$K_d \sim 4.2$ and 6.8 nM in the presence of AMPPNP and ADP, respectively (see ref 16)], one can derive ΔG_{exp} values of approximately −11.6 and −11.3 kcal/mol in the ATP and ADP states, respectively.

Computational Alanine-Scanning Mutagenesis Based on Kinesin−MT Binding Free Energy Calculation. The computational alanine-scanning protocol is a widely used method for evaluating the contributions of individual residue side chains to protein−protein or protein−ligand binding free energy.[41−51] This protocol is performed as follows. (1) We extract 100 snapshots of the last 10 ns of the MD trajectory of the wild-type kinesin−MT complex (after stripping all waters and ions). (2) For each snapshot, we computationally mutate each charged residue of kinesin to alanine (following ref 42). (3) For each snapshot, we calculate kinesin−MT binding free energy ΔG (see below) for both the wild type (ΔG_{wt}) and each alanine mutant (ΔG_{mut}). The difference in ΔG ($\Delta\Delta G = \Delta G_{mut} - \Delta G_{wt}$) is used to evaluate the contribution of each charged residue to kinesin−MT binding. (4) For each mutant, we calculate the average ($\Delta\Delta G_{avg}$) and standard error ($\Delta\Delta G_{std}$) of the $\Delta\Delta G$ values for 100 snapshots and then select those important residues with statistically significant $\Delta\Delta G$ values that satisfy the relationship $|\Delta\Delta G_{avg}|/\Delta\Delta G_{std} > 1$.

Following early studies,[62−65] the same MD trajectory of the wild-type kinesin−MT complex is used to extract snapshots of unbound kinesin, unbound MT, the kinesin−MT complex, and their mutants. Because of a reduction in statistical uncertainty and the cancellation of errors in the ΔG calculation, such a single-trajectory-based protocol was shown to be more efficient and accurate than running separate MD trajectories for bound and unbound proteins and their mutants.[66−68]

In this study, the kinesin−MT binding free energy is calculated using a continuum solvent model (following ref 69). The binding free energy ΔG is expressed as $\Delta G_{np} + \Delta G_{elec}$. Here the nonpolar contribution ΔG_{np} ($=\alpha E_{vdW}$) is empirically written as a fraction ($\alpha < 1$) of the van der Waals (VDW) interaction energy E_{vdW} between kinesin and MT, and the electrostatic contribution ΔG_{elec} ($=\beta\Delta E_{elec}$) is empirically written as a fraction ($\beta < 1$) of the change in electrostatic energy ΔE_{elec} from unbound kinesin and MT to the kinesin−MT complex. E_{elec} is calculated using the Poisson−Boltzmann (PB) method.[70,71] An α of 0.158 and a β of 0.153 are optimized by minimizing the root-mean-square error between calculated $\Delta\Delta G$ and experimental $\Delta\Delta G_{exp}$ (see above). α is small because the gain in favorable VDW interaction energy between kinesin and MT is largely compensated by the loss of VDW interaction energy between free proteins and water ($\alpha = 0.17$ was obtained in ref 69). β is small because the PB calculation based on a single MD trajectory generally overestimates solvation and interaction energies[72] of charged residues that are involved in buried salt bridges or hydrogen bonds;[42,64] these residues are likely to undergo significant structural relaxation upon mutation.[62] An alternative way to correct such overestimation is to use a large dielectric constant for the protein interior,[43,69,70,73−77] which may however result in inconsistent treatments of electrostatic contributions from charged and uncharged residues.[74,75,77] For the PB calculation,[70,71] a dielectric constant ε of 4 is used for the protein interior,[76,78−80] which accounts for some dielectric response due to structural changes not treated explicitly. An ε of 4 can also be obtained on the basis of the measurement of dry proteins and peptide powders.[78,81] A dielectric constant of 80 is used for the exterior aqueous environment. A probe radius of 1.4 Å is used to define the molecular surface corresponding to the dielectric boundary. The salt concentration is set to 40 mM, corresponding to the buffer condition for kinetic measurements.[1] All the PB calculations are performed using the PBEQ module[71,82,83] of CHARMM.[84] Each PB calculation is conducted by using the bilinear interpolation to construct the boundary potential. The atomic Born radii used here were previously calibrated and optimized to reproduce the electrostatic free energy of the 20 amino acids in MD simulations with explicit water molecules.[83] Following previous studies,[41−43,62,67,85] the entropic contribution to ΔG is ignored because our goal is to estimate the relative binding free energy ($\Delta\Delta G$) for structurally similar complexes (i.e., wild type and mutants) whose entropy contribution largely cancels out.

Optimization and Evaluation of the Calculated Mutational Change in Binding Free Energy $\Delta\Delta G$. We scan α and β values within the range of 0−1 to minimize the following root-mean-square error (rmse) between the calculated $\Delta\Delta G$

and experimental $\Delta\Delta G_{exp}$: rmse = $[1/N\sum_n(\Delta\Delta G_n - \Delta\Delta G_{exp,n})^2]^{1/2}$, where $\Delta\Delta G_n$ ($\Delta\Delta G_{exp,n}$) is the calculated $\Delta\Delta G$ (experimental $\Delta\Delta G_{exp}$) of residue n and $N = 20$ is the number of charged residues of KHC with $\Delta\Delta G_{exp}$ measured.[1]

The overall fitting quality is assessed by the coefficient of multiple determination R^2 (see ref 86): $R^2 = 1 - [\sum_n(\Delta\Delta G_n - \Delta\Delta G_{exp,n})^2]/[\sum_n(\Delta\Delta G_{exp,n} - \Delta\Delta G_{exp,avg})^2]$, where $\Delta\Delta G_{exp,avg}$ is the average of the experimental $\Delta\Delta G_{exp}$.

To assess possible overfitting, the cross-validated statistical figure of merit, Q_{loo}^2, is calculated as follows: $Q_{loo}^2 = 1 - [\sum_n(\Delta\Delta G_n^* - \Delta\Delta G_{exp,n})^2]/[\sum_n(\Delta\Delta G_{exp,n} - \Delta\Delta G_{exp,avg})^2]$, where $\Delta\Delta G_n^*$ is calculated using the optimal parameters for the data set with $\Delta\Delta G_{exp,n}$ excluded, so Q_{loo}^2 gives a measure of the model's predictive power.

Residue Conservation Analysis. We use precalculated residue conservation scores from ConSurf-DB (http://consurfdb.tau.ac.il/) to assess residue conservation in the kinesin superfamily. We use the ConSurf server (http://consurf.tau.ac.il/)[87−89] to align multiple sequences of kinesin 1 and kinesin 3 families and assess residue conservation in each family. The kinesin sequences are obtained from the Kinesin Homepage (http://www.cellbio.duke.edu/kinesin/MotorSeqTable.html). The residue positions with a conservation grade of ≥7 are deemed to be conserved.

RESULTS AND DISCUSSION

Equilibration of the MD Simulation. We have built three all-atom models of the kinesin−MT complex [KHC_{ADP}, $KIF1A_{ADP}$, and $KIF1A_{ATP}$ (see Methods)] comprised of a kinesin (KHC or KIF1A) and two tubulins (α- and β-tubulin), which are optimized by energy minimization followed by 30 ns MD simulations with explicit solvents (see Methods). The root-mean-square deviation (rmsd) of all backbone atoms (with respect to the initial models) slowly increases during the simulations, suggesting that the entire kinesin−MT complex undergoes slow structural relaxation (see Figure 2). Nevertheless, the rmsd restricted to the kinesin−MT interface (as defined in ref 90) is smaller and more stable during most of the simulations (see Figure 2), so we postulate that the kinesin−MT dynamic interaction has reached an equilibrium state during the last 10 ns of MD simulations, which allows the calculation of the kinesin−MT binding free energy (see below).

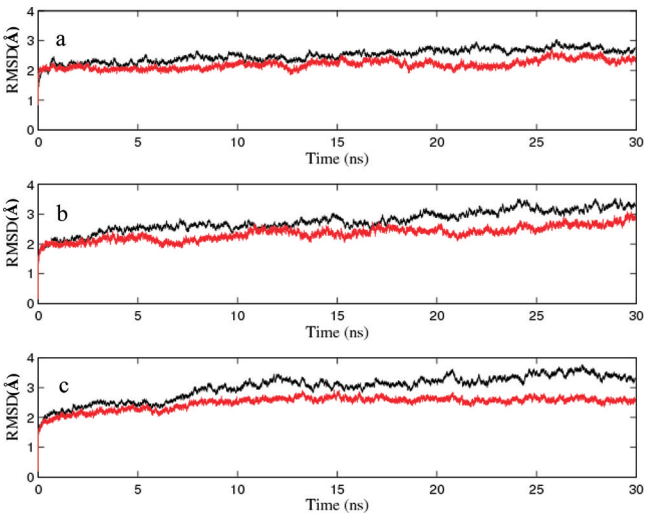

Figure 2. Backbone rmsd (with respect to the initial models) of all residues (black) and kinesin−MT interface residues (red) in (a) KHC_{ADP}, (b) $KIF1A_{ADP}$, and (c) $KIF1A_{ATP}$ as a function of simulation time.

Calculation of the Kinesin−MT Binding Free Energy. We initially used the MM-PBSA (molecular mechanics−Poisson−Boltzmann surface area) method[62,91] to calculate the kinesin−MT binding free energy (ΔG) and its change caused by alanine mutation ($\Delta\Delta G$), which gave significantly overestimated $\Delta\Delta G$ values compared with experimental ones. This overestimation is probably due to inadequate structural relaxation in the MM-PBSA calculation based on a single MD trajectory.[62] To fully account for structural relaxation, one can run separate MD simulations for unbound and bound proteins and their mutants, which will not only increase the computing cost dramatically but also introduce large statistical error into the free energy calculation. To allow accurate and efficient calculation of the kinesin−MT binding free energy, we have adopted an empirical method that calculates ΔG as a linear combination of two contributions: the kinesin−MT VDW interaction energy (calculated by MM force field) and the change in electrostatic free energy upon binding [calculated by the PB method (see Methods)]. The corresponding coefficients [$\alpha = 0.158$ (for the VDW contribution) and $\beta = 0.153$ (for the electrostatic contribution)] are determined by fitting the experimental $\Delta\Delta G_{exp}$ (see Methods). This empirical method is akin to the linear interaction energy method (LIE),[92,93] which calculates protein−ligand binding free energy by linearly combining electrostatic and VDW energies between the ligand and its surroundings. Similar to this study, several LIE-based studies also yielded small β values of ≤0.2 for the electrostatic contribution.[94−96] Similarly, in an early PB-based calculation of $\Delta\Delta G$ of 10 lysozyme mutants, it was found that the electrostatic contribution should be reduced by 0.4 to fit the experimental $\Delta\Delta G$ data.[97] The idea of linearly combining various terms of MM-PBSA was also explored recently.[98]

To calculate kinesin−MT binding free energy ΔG in KHC_{ADP} and $KIF1A_{ATP}$, we used 100 snapshots from the last 10 ns of MD trajectories (for $KIF1A_{ADP}$, only 80 snapshots are used because ΔG shows drift during the last 2 ns of MD simulation). To check the stability of ΔG values over time (10 ns for KHC_{ADP} and $KIF1A_{ATP}$ and 8 ns for $KIF1A_{ADP}$), we performed linear regression that yields negligible slopes: 4.3×10^{-4}, 2.8×10^{-4}, and 6.4×10^{-4} kcal mol^{-1} ps^{-1} for KHC_{ADP}, $KIF1A_{ADP}$, and $KIF1A_{ATP}$, respectively, which are comparable with low values (2×10^{-3} kcal mol^{-1} ps^{-1}) reported in a previous study.[45]

We have calculated the average ΔG (ΔG_{avg}) for three kinesin−MT systems (approximately −23.2, −30.0, and −29.4 kcal/mol for KHC_{ADP}, $KIF1A_{ADP}$, and $KIF1A_{ATP}$, respectively). Estimation based on experimental data gives ΔG_{exp} values of approximately −6.8, −11.3, and −11.6 kcal/mol for the ADP state of KHC and the ADP and ATP states of KIF1A, respectively (see Methods). The shift of 16−19 kcal/mol between calculated and experimental ΔG values can be attributed to entropy loss upon kinesin−MT binding, which is not included in our calculation [the rotational and translational entropy loss upon binding was estimated to be 7−15 kcal/mol (see ref 99)]. The calculation described above explains the experimental finding of a higher MT binding affinity for KIF1A than for KHC in the ADP state, which underlies the unique ability of KIF1A to undergo processive diffusion along MT for many steps without dissociation.[17] We note that our MD simulation is too short to explore the

diffusive motion of KIF1A along MT, and it can only probe the affinity of KIF1A for MT while it binds transiently with a tubulin dimer. It is possible that a different affinity would be obtained if diffusion could be properly modeled.

We have performed a breakdown of ΔG to electrostatic (−4.0, −7.9, and −9.0 kcal/mol for KHC_{ADP}, $KIF1A_{ADP}$, and $KIF1A_{ATP}$, respectively) and VDW (−19.2, −22.1, and −20.4 kcal/mol for KHC_{ADP}, $KIF1A_{ADP}$, and $KIF1A_{ATP}$, respectively) contributions. The kinesin−MT binding free energy is found to be dominated by the VDW contribution (including the nonpolar part of the solvation free energy). The electrostatic contribution (including the polar part of the solvation free energy), although relatively small, can still play an important role in kinesin−MT binding. In fact, the electrostatic contribution is more important than the VDW contribution in determining the difference in ΔG between two kinesins—the electrostatic (VDW) contribution to the difference in ΔG between KHC_{ADP} and $KIF1A_{ADP}$ is 3.9 (2.9) kcal/mol. The small electrostatic contribution is due to the cancellation of favorable electrostatic interactions between oppositely charged residues of kinesin and MT by the unfavorable solvation energy of charged residues.[100−102] Although the net contribution of electrostatic interactions to the protein assembly process is generally expected to be unfavorable, favorable electrostatic binding free energy may arise when the partner proteins have a complementary charge distribution (see refs 72 and 90), which may result from evolutionary optimization of binding affinity.[103]

Comparison with Experimental Alanine-Scanning Mutagenesis Results. To further probe the kinesin−MT interactions at the residue level of detail, we performed computational alanine-scanning mutagenesis on all charged residues of kinesin (see Methods). The contribution of each charged residue's side chain to kinesin−MT binding is quantified by calculating the change in kinesin−MT binding free energy ($\Delta\Delta G$) caused by its mutation to alanine (see Methods). Furthermore, we have performed a breakdown of $\Delta\Delta G$ into VDW and electrostatic contributions for each charged residue of kinesin, which suggests a larger contribution of electrostatic than VDW interaction for these residues (see Table S1 of the Supporting Information).

In an experimental alanine-scanning mutagenesis study, 36 alanine mutants of KHC were characterized using ATPase assays.[1] Experimental $\Delta\Delta G_{exp}$ values for alanine mutations can be estimated from the measurements of the apparent Michaelis−Menten constant for microtubule-dependent ATPase activation (K_{mMT}) and the maximal ATP turnover rate (k_{cat}) (see Methods). We have found that the calculated $\Delta\Delta G$ values are in excellent agreement with experimental $\Delta\Delta G_{exp}$ values with an rmse of 0.35 kcal/mol and an R^2 of 0.72 (see Figure 3). To check for possible overfitting, we redo the optimization of α and β after leaving one $\Delta\Delta G_{exp}$ value (for residue n) out, and then we recalculate $\Delta\Delta G$ for residue n. In this way, we have obtained a cross-validated statistical figure of merit ($Q_{loo}^2 = 0.67$) and a leave-one-out cross-validated rmse of 0.38 kcal/mol, which are close to the R^2 and rmse obtained by fitting all $\Delta\Delta G_{exp}$ data. Therefore, our $\Delta\Delta G$ calculation based on optimized parameters ($\alpha = 0.158$, and $\beta = 0.153$) has good predictivity and gives a statistically robust result.

To further test the predictivity of our $\Delta\Delta G$ calculation, we calculated $\Delta\Delta G$ for 16 uncharged residues of KHC probed in ref 1 (using the model parameters optimized for charged kinesin residues). Among these uncharged residues, we have identified Y274 and L248 as the top two most important for kinesin−MT binding (ranked by $\Delta\Delta G$, which is 1.24 kcal/mol for Y274 and 0.92 kcal/mol for L248). Encouragingly, the same two residues were identified by experimental alanine-scanning mutagenesis[1] as the top two most important for kinesin−MT binding (ranked by $\Delta\Delta G_{exp}$ which is 0.87 kcal/mol for Y274 and 0.86 kcal/mol for L248). Additionally, R278 is identified as the most important charged residue for kinesin−MT binding both computationally and experimentally (see Table 1). Therefore, our $\Delta\Delta G$ calculation can correctly identify both charged and uncharged residues critically involved in kinesin−MT binding.

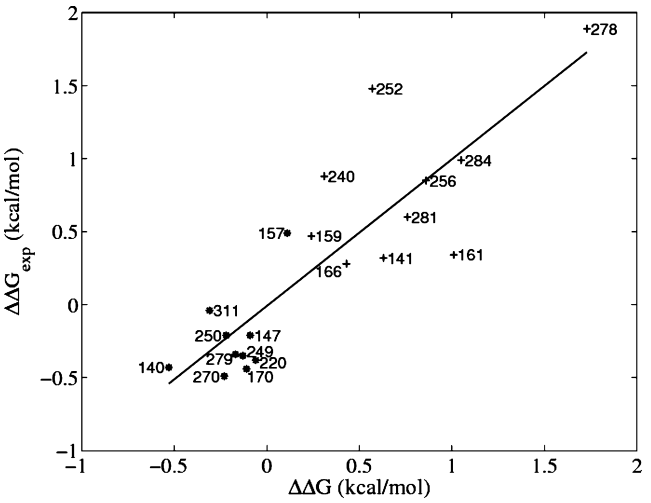

Figure 3. Calculated $\Delta\Delta G$ values and experimental $\Delta\Delta G_{exp}$ values for 20 charged residues of KHC.[1] Plus signs denote data for positively charged residues, and asterisks denote data for negatively charged residues. The straight line shows the result of linear fitting: $\Delta\Delta G_{exp} = -0.009 + 1.004\Delta\Delta G$.

Next, we use $\Delta\Delta G$ values to sort all charged residues of kinesin and then select those residues with large positive or negative $\Delta\Delta G$ values (see Table 1), which are predicted to be involved in strengthening or weakening kinesin−MT binding, respectively. We will focus our discussion on these residues.

Positively Charged Residues Involved in Strengthening Kinesin−MT Binding. A number of positively charged residues are predicted to be important in strengthening kinesin−MT binding, which are distributed in several secondary structural elements of kinesin (see Figure 1), including loop L2 (K41, K44, and K48 of KIF1A), loop L7 (K141 and R143 of KHC and R153 of KIF1A), loop L8 (K159, R161, and K166 of KHC and K163, R167, and R169 of KIF1A), switch I (R203 of KHC and R216 of KIF1A), loop L11 (K237, K240, and K252 of KHC and R254, K261, R264, and K266 of KIF1A), helix α4 (K256 of KHC and K273 and K280 of KIF1A), loop L12 (R278 of KHC and K294, K296, K297, K298, K299, K300, and R307 of KIF1A), helix α5 and loop L13 (K281 and R284 of KHC and R316 of KIF1A), and helix α6 (K313 and R321 of KHC and R346 and R350 of KIF1A).

To offer structural insights into the kinesin−MT interactions involving the charged residues mentioned above, we calculated an average structure for each system from the last 10 ns of the MD trajectory. On the basis of the average structure, we define that two charged residues form electrostatic interaction if their charged side chain atoms (NZ of Lys, NH1 and NH2 of Arg, OE1 and OE2 of Glu, and OD1 and OD2 of Asp) are within 10

dx.doi.org/10.1021/bi2008257 | Biochemistry 2011, 50, 8645−8655

Table 1. Mutational Changes in Kinesin−MT Binding Free Energy ($\Delta\Delta G_{avg}$) of Selected Charged Residues in KHC_{ADP}, $KIF1A_{ADP}$, and $KIF1A_{ATP}$[a]

KHC_{ADP}		$KIF1A_{ADP}$		$KIF1A_{ATP}$		$KIF1A_{ADP}$ − $KIF1A_{ATP}$	
residue number	$\Delta\Delta G_{avg}$ (kcal/mol)	residue number	$\Delta\Delta G_{avg}$ (kcal/mol)	residue number	$\Delta\Delta G_{avg}$ (kcal/mol)	residue number	$\Delta\Delta G_{avg}$ (kcal/mol)
R278*	1.73 [1.89]	R346*	1.93	K261	1.85	K44	1.42
K237*	1.41	K44	1.73	K297	1.49	R346	1.25
R284̂	1.05 [0.99]	K48	1.31	R169*	1.11	K48	0.71
R161	1.01 [0.34]	R307* (278)	1.24	R307* (278)	1.01	K296	0.56
R321*	0.99	K296̂	1.18	K280*	0.95	D256	0.38
K313	0.92	R350* (321)	1.09	E267* (250)	0.86	R350	0.31
K256*	0.86 [0.85]	R169*	0.99	K273̂ (256)	0.82	K300	0.31
K281*	0.76 [0.60]	K266̂	0.96	R350* (321)	0.78	K294	0.30
K141	0.63 [0.32]	K261	0.93	R167	0.75		
K252̂	0.57 [1.48]	K273̂ (256)	0.82	K41	0.74		
K166	0.43 [0.28]	K280*	0.66	K266̂	0.72	K297	−1.25
K44	0.42	K300	0.64	R153 (141)	0.69	E267	−1.06
R203*	0.32	R167	0.63	R346*	0.69	K261	−0.92
K240*	0.31 [0.88]	K298	0.62	K298	0.66	R254	−0.53
K159̂	0.24 [0.47]	K41	0.58	R254* (237)	0.65	R153	−0.35
R143	0.21	R316*	0.46	K296̂	0.61	R216	−0.30
		K294̂	0.45	K48	0.59	K280	−0.29
D140*	−0.53 [−0.43]	K299	0.44	R216* (203)	0.47		
E309	−0.34	R153 (141)	0.34	R316*	0.34		
E311*	−0.31 [−0.04]	R264*	0.31	K300	0.33		
E270	−0.23 [−0.49]	K297	0.24	K44	0.32		
E199̂	−0.23			R264*	0.27		
E250*	−0.22 [−0.21]	D339	−0.60	K299	0.25		
E236*	−0.20	E170* (157)	−0.40	R18	0.23		
		E45	−0.39	K163 (K150)	0.19		
		D349	−0.39				
		E152* (140)	−0.31	D339	−0.69		
		E340* (311)	−0.27	D256	−0.59		
		D308* (279)	−0.25	E340* (311)	−0.45		
		E287 (270)	−0.24	E152* (140)	−0.41		
		D256	−0.21	E253* (236)	−0.38		
		E267* (250)	−0.20	E170* (157)	−0.32		
		E179 (170)	−0.19	D308* (279)	−0.27		
				E179 (170)	−0.21		

[a]We select charged residues of kinesin for which $|\Delta\Delta G_{avg}|/\Delta\Delta G_{std} > 1$, where $\Delta\Delta G_{std}$ is 0.19−0.20 for KHC_{ADP}, 0.18−0.19 for $KIF1A_{ADP}$, and 0.19−0.20 for $KIF1A_{ATP}$ and 0.26−0.27 for the difference between $KIF1A_{ADP}$ and $KIF1A_{ATP}$. The experimental $\Delta\Delta G_{exp}$ values are enclosed in brackets. The KHC residue numbers corresponding to some KIF1A residues are enclosed in parentheses. Residues marked with an asterisk are conserved in the kinesin superfamily. Residues marked with a caret are conserved in the kinesin 1 or kinesin 3 family.

Å of each other, and two oppositely charged residues form a salt bridge interaction if their charged side chain atoms are within 4 Å of each other (see ref 104). Most of the charged residues mentioned above form favorable electrostatic interactions with MT residues in the average structures. For example, K41 of loop L2 interacts with E155, E196, and R156 of α-tubulin in $KIF1A_{ADP}$ (Figure S2a of the Supporting Information) and with E196, D424, and R264 of α-tubulin in $KIF1A_{ATP}$ (Figure S3a of the Supporting Information). K141 of loop L7 interacts with E159 and E196 of β-tubulin in KHC_{ADP} (Figure S1a of the Supporting Information). R161 of loop L8 interacts with E420, E422, D427, and R400 of β-tubulin in KHC_{ADP} (Figure S1b of the Supporting Information). K237 of loop L11 interacts with E414, E417, and K112 of α-tubulin in KHC_{ADP} (Figure S1c of the Supporting Information). K256 of helix α4 interacts with E196, R158, and R264 of β-tubulin in KHC_{ADP} (Figure S1d of the Supporting Information). R278 of loop L12 interacts with E196, E420, E422, D427, E431, and R264 of β-tubulin in KHC_{ADP} (Figure S1e of the Supporting Information). K281 of helix α5 and loop L13 interacts with E159, E196, and E420 of β-tubulin in KHC_{ADP} (Figure S1f of the Supporting Information). K313 of helix α6 interacts with E420 and E423 of α-tubulin in KHC_{ADP} (Figure S1g of the Supporting Information).

Interestingly, some of these charged residues interact differently with MT in $KIF1A_{ADP}$ and $KIF1A_{ATP}$.

In loop L2, K44 interacts with E196, E417, E420, E423, and D424 of α-tubulin to form 10 opposite-charge atom pairs (within 10 Å, same as below) in $KIF1A_{ADP}$ (Figure S2a of the Supporting Information) and with D431, E434, and K430 of α-tubulin to form only four opposite-charge atom pairs and one same-charge pair in $KIF1A_{ATP}$ (Figure S3a of the Supporting Information). Therefore, K44 of loop L2 favors MT binding in the ADP state over the ATP state [with a $\Delta\Delta G$ difference of 1.42 kcal/mol (see Table 1)]. Indeed, previous EM studies showed the proximity of loop L2 to MT in both KIF1A[53] and

NCD[22] in the ADP state. In contrast, loop L2 of KHC is very short and thus contributes little to kinesin−MT binding.

In loop L8, R167 is involved in MT binding in both ADP and ATP states [with a $\Delta\Delta G$ difference of 0.12 kcal/mol (see Table 1)]; it interacts with E196, E417, and E420 of β-tubulin in $KIF1A_{ADP}$ (Figure S2b of the Supporting Information) and with D414, E417, and E420 of β-tubulin in $KIF1A_{ATP}$ (Figure S3b of the Supporting Information). A nearby residue, R169, also binds MT strongly in the ATP and ADP states [with a $\Delta\Delta G$ difference of 0.12 kcal/mol (see Table 1)]. Therefore, loop L8 is involved in MT binding in ADP and ATP states, which agrees with a mutational study of L8 residues (K161A/R167A/R169A/K183A).[16]

In the switch I region (near loop L9), R216 interacts with E414 of α-tubulin in $KIF1A_{ATP}$ (Figure S3c of the Supporting Information) but forms no electrostatic interaction with MT in $KIF1A_{ADP}$. This interaction in the ATP state may allow MT binding to trigger displacement of switch I toward MT that causes the closing of the active site as found by EPR spectroscopy.[38,105] Interestingly, the R598A mutant of Kar3 (corresponding to R216 of KIF1A) was found to exhibit no MT-activated ATPase activity in steady state assays and bind weakly to MT in the presence of ADP or in the absence of nucleotide.[106]

In loop L11, R254 interacts with E155, E414, E417, and K112 of α-tubulin in $KIF1A_{ATP}$ (Figure S3d of the Supporting Information) and forms no electrostatic interaction with MT in $KIF1A_{ADP}$. Similarly, K261 interacts favorably with E414 and E417 of α-tubulin in $KIF1A_{ATP}$ (Figure S3d of the Supporting Information) and with E97 of α-tubulin and D163 of β-tubulin, but unfavorably with R105 of α-tubulin in $KIF1A_{ADP}$ (Figure S2c of the Supporting Information). Therefore, R254 and K261 favor MT binding in the ATP state over the ADP state [with $\Delta\Delta G$ difference values of 0.53 and 0.92 kcal/mol (see Table 1)], suggesting that loop L11 is involved in MT binding in the ATP state more than in the ADP state, which agrees with the previous finding that mutations of L11 residues (K261A/R264A/K266A) affect affinity in the ATP state more than in the ADP state.[16]

In loop L12 (including K loop of KIF1A), K296 interacts with D437, D441, E442, and E445 of β-tubulin to form seven opposite-charge atom pairs in $KIF1A_{ADP}$ (Figure S2d of the Supporting Information) and with D396, E420, E423, and R422 of α-tubulin to form five opposite-charge atom pairs and two same-charge atom pairs in $KIF1A_{ATP}$ (Figure S3e of the Supporting Information). Therefore, K296 favors MT binding in the ADP state over the ATP state [with a $\Delta\Delta G$ difference of 0.56 kcal/mol (see Table 1)]. In the average structures of the KIF1A−MT complex, loop L12 and K loop extend farther into MT in the ADP state than in the ATP state (see Figure 1b,c), which agrees with the previous finding that mutations of K loop lysines affect affinity in the ADP state more than in the ATP state.[107]

In helix α6, R346 interacts with E415, E420, E423, D424, and R402 of α-tubulin in $KIF1A_{ADP}$ (Figure S2e of the Supporting Information) and with only E420 and E423 of α-tubulin in $KIF1A_{ATP}$ (Figure S3f of the Supporting Information). R350 interacts with E414, E415, E420, and R402 of α-tubulin in $KIF1A_{ATP}$ (Figure S3f of the Supporting Information) and with E415, K401, and R402 of α-tubulin in $KIF1A_{ADP}$ (Figure S2e of the Supporting Information). R346 and R350 favor MT binding in the ADP state versus the ATP state [with $\Delta\Delta G$ difference values of 1.25 and 0.31 kcal/mol, respectively (see Table 1)], so helix α6 is likely involved in MT binding in the ADP state more than in the ATP state.

Taken together, the structural observations described above agree with our finding of different $\Delta\Delta G$ values for the residues mentioned above in $KIF1A_{ATP}$ and $KIF1A_{ADP}$ (see Table 1). These residues are therefore predicted to critically regulate the different MT binding affinity between the ADP and ATP states.

The importance of the charged residues mentioned above is supported by residue conservation analysis based on multiple-sequence alignment (see Methods). Among these residues, K237, K240, K256, K278, K281, and R321 of KHC and R169, R216, R254, R264, K280, R307, R316, R346, and R350 of KIF1A are conserved in the kinesin superfamily. K159, K252, and R284 of KHC are conserved in the kinesin 1 family. K266, K273, K294, and K296 of KIF1A are conserved in the kinesin 3 family.

Negatively Charged Residues Involved in Weakening of Kinesin−MT Binding. A number of negatively charged residues are predicted to be involved in weakening kinesin−MT binding, which are distributed in several key structural motifs of kinesin (see Figure 1), including loop L2 (E45 of KIF1A), loop L7 (D140 of KHC and E152 of KIF1A), loop L8 (E170 and E179 of KIF1A), switch I (E199 of KHC), loop L11 (E236 and E250 of KHC and E253, D256, and E267 of KIF1A), helix α4 (E270 of KHC and E287 of KIF1A), loop L12 (D308 of KIF1A), helix α6 (E309 and E311 of KHC and D339, E340, and D349 of KIF1A).

Most of these residues form unfavorable electrostatic interactions with MT residues in the average structures. For example, D140 of loop L7 interacts with E159, E196, and R158 of β-tubulin in KHC_{ADP} (Figure S1a of the Supporting Information); E236 of loop L11 interacts with E414 of α-tubulin in KHC_{ADP} (Figure S1c of the Supporting Information), and E309 of helix α6 interacts with E420 of α-tubulin in KHC_{ADP} (Figure S1g of the Supporting Information).

Interestingly, some of these charged residues interact differently with MT in $KIF1A_{ADP}$ and $KIF1A_{ATP}$. For example, in loop L11, E267 interacts with E97, D98, E113, E411, K96, and R105 of α-tubulin and D163, R164, and R253 of β-tubulin in $KIF1A_{ATP}$ (Figure S3g of the Supporting Information) but forms no electrostatic interaction with MT in $KIF1A_{ADP}$. Therefore, E267 favors kinesin−MT binding in the ATP state over the ADP state [with a $\Delta\Delta G$ difference of 1.06 kcal/mol (see Table 1)], which further contributes to the high affinity in the ATP state together with those positively charged residues of loop L11.

The importance of these charged residues is supported by residue conservation analysis (see Methods). Among these residues, D140, E311, E236, E250 of KHC, E152, E170, E253, E267, D308, and E340 of KIF1A are conserved in the kinesin superfamily.

The importance of the charged residues mentioned above is also supported by previous mutational studies. The E164A mutant of *Drosophila melanogaster* kinesin (corresponding to E170 of KIF1A) was found to exhibit reduced steady state ATPase activity and higher affinity for MT.[108] The E236A mutant of KHC (corresponding to E253 of KIF1A) was shown to have very low ATPase activities in the presence of MT.[109] The mutation of E237 of rat KHC (corresponding to E253 of KIF1A) reduced or abolished MT-dependent ATPase activity.[110] The E631A mutant of Kar3 (corresponding to E253 of KIF1A) was shown to exhibit no MT-activated ATPase activity in steady state assays and bind tightly to MT in the

dx.doi.org/10.1021/bi2008257 | *Biochemistry* 2011, 50, 8645−8655

presence of ADP or in the absence of nucleotide.[106] The E311A mutant of KHC was found to show a ~3-fold reduction in both MT gliding velocity and MT-stimulated ATPase activity.[111]

Interactions between Kinesin and the E-Hook of MT. Finally, we discuss the kinesin−MT interactions involving the C-terminal E-hook of tubulins (residues 440−451 of α-tubulin and 438−455 of β-tubulin). In the average structure of $KIF1A_{ADP}$, E45 of loop L2 interacts with E443 of α-tubulin (see Figure S2a of the Supporting Information) and D289, K296, and K299 of loop L12 interact with D441, E442, and E445 of β-tubulin (see Figure S2d of the Supporting Information). No electrostatic interactions are formed between the E-hook and kinesin in the other two systems. Our finding supports the proposal that the interaction between loop L12 and the E-hook allows diffusive binding of KIF1A in the ADP state,[16] and this interaction does not contribute to the strong MT-binding state like the ATP state.[107]

CONCLUSION

To develop a detailed understanding of kinesin−MT binding in structural and energetic terms, we have performed an extensive alanine-scanning mutagenesis study of all charged residues of three kinesin models (ADP-bound KHC and ADP-bound and ATP-bound KIF1A). This study is based on three 30 ns MD simulations of kinesin−MT systems in ADP and ATP states. To the best of our knowledge, these simulations are the longest ever performed for the kinesin−MT complex with explicit solvents. Although the kinesin kinetics (approximately milliseconds) remains beyond the reach of all-atom MD simulations, far less simulation time may suffice for free energy calculation based on the sampling of conformational fluctuations near a stable state (such as the ADP state and the ATP state).

On the basis of the MD simulations, we have calculated the kinesin−MT binding free energy (ΔG) and its mutational changes ($\Delta\Delta G$). The latter are in excellent agreement with results of an experimental alanine-scanning study.[1] Furthermore, on the basis of the ranking of $\Delta\Delta G$ values, we have predicted a key set of positively and negatively charged residues of kinesin involved in strengthening and weakening kinesin−MT binding, respectively. These charged residues form intricate networks of hydrogen bonds and salt bridges at the kinesin−MT interface, which make an overall favorable contribution to kinesin−MT binding.[90] Many of the predicted key residues are strongly conserved or previously found to be important in mutational studies.[1,15,16,106,107,110−112] Some of them (in loops L2, L11, and L12) contribute to MT binding in a nucleotide state-dependent manner, giving rise to high and low affinity in the ADP and ATP states, respectively. Some of them (in loop L2 and K loop) contribute to MT binding in some kinesins (such as KIF1A) but not in others. Collectively, these charged residues may modulate the kinesin−MT binding affinity according to the functional roles of various kinesins. This study will offer promising targets for future mutational and functional studies for probing the motor mechanisms of kinesin and engineering of kinesins with novel motor properties.

ASSOCIATED CONTENT

Supporting Information

Breakdown of electrostatic ($\Delta\Delta G_{elec}$) and van der Waals ($\Delta\Delta G_{VDW}$) contributions to $\Delta\Delta G$ for selected charged residues in KHC_{ADP}, $KIF1A_{ADP}$, and $KIF1A_{ATP}$ (Table S1) and electrostatic interactions involving the charged residues in key secondary structural elements of KHC_{ADP}, $KIF1A_{ADP}$, and $KIF1A_{ATP}$ (Figures S1−S3). This material is available free of charge via the Internet at http://pubs.acs.org.

AUTHOR INFORMATION

Corresponding Author

*E-mail: wjzheng@buffalo.edu. Telephone: (716) 645-2947. Fax: (716) 645-2507.

Funding

Supported by the American Heart Association (Grant 0835292N) and the National Science Foundation (Grant 0952736).

ABBREVIATIONS

MT, microtubule; MD, molecular dynamics; P_i, inorganic phosphate; EM, electron microscopy; KHC, human conventional kinesin; VDW, van der Waals; PME, particle mesh Ewald; PB, Poisson−Boltzmann; rms, root-mean-square; rmsd, root-mean-square deviation; MM-PBSA, molecular mechanics−Poisson−Boltzmann surface area; LIE, linear interaction energy method.

REFERENCES

(1) Woehlke, G., Ruby, A. K., Hart, C. L., Ly, B., Hom-Booher, N., and Vale, R. D. (1997) Microtubule interaction site of the kinesin motor. *Cell 90*, 207−216.

(2) Hirokawa, N. (1998) Kinesin and dynein superfamily proteins and the mechanism of organelle transport. *Science 279*, 519−526.

(3) Valentine, M. T., Fordyce, P. M., and Block, S. M. (2006) Eg5 steps it up! *Cell Div. 1*, 31.

(4) Tucker, C., and Goldstein, L. S. (1997) Probing the kinesin-microtubule interaction. *J. Biol. Chem. 272*, 9481−9488.

(5) Lawrence, C.J., Dawe, R. K., Christie, K. R., Cleveland, D. W., Dawson, S. C., Endow, S. A., Goldstein, L. S., Goodson, H. V., Hirokawa, N., Howard, J., Malmberg, R. L., McIntosh, J. R., Miki, H., Mitchison, T. J., Okada, Y., Reddy, A. S., Saxton, W. M., Schliwa, M., Scholey, J. M., Vale, R. D., Walczak, C. E., and Wordeman, L. (2004) A standardized kinesin nomenclature. *J. Cell Biol. 167*, 19−22.

(6) Miki, H., Okada, Y., and Hirokawa, N. (2005) Analysis of the kinesin superfamily: Isights into structure and function. *Trends Cell Biol. 15*, 467−476.

(7) Case, R. B., Rice, S., Hart, C. L., Ly, B., and Vale, R. D. (2000) Role of the kinesin neck linker and catalytic core in microtubule-based motility. *Curr. Biol. 10*, 157−160.

(8) Vale, R. D., Case, R., Sablin, E., Hart, C., and Fletterick, R. (2000) Searching for kinesin's mechanical amplifier. *Philos. Trans. R. Soc. London, Ser. B 355*, 449−457.

(9) Valentine, M. T., and Gilbert, S. P. (2007) To step or not to step? How biochemistry and mechanics influence processivity in Kinesin and Eg5. *Curr. Opin. Cell Biol. 19*, 75−81.

(10) Gilbert, S. P., Webb, M. R., Brune, M., and Johnson, K. A. (1995) Pathway of processive ATP hydrolysis by kinesin. *Nature 373*, 671−676.

(11) Ma, Y. Z., and Taylor, E. W. (1997) Kinetic mechanism of a monomeric kinesin construct. *J. Biol. Chem. 272*, 717−723.

(12) Moyer, M. L., Gilbert, S. P., and Johnson, K. A. (1998) Pathway of ATP hydrolysis by monomeric and dimeric kinesin. *Biochemistry 37*, 800−813.

(13) Cross, R. A. (2004) The kinetic mechanism of kinesin. *Trends Biochem. Sci. 29*, 301−309.

(14) Hackney, D. D. (1988) Kinesin ATPase: Rate-limiting ADP release. *Proc. Natl. Acad. Sci. U.S.A. 85*, 6314−6318.

(15) Rice, S., Lin, A. W., Safer, D., Hart, C. L., Naber, N., Carragher, B. O., Cain, S. M., Pechatnikova, E., Wilson-Kubalek, E. M., Whittaker, M., Pate, E., Cooke, R., Taylor, E. W., Milligan, R. A., and Vale, R. D.

(1999) A structural change in the kinesin motor protein that drives motility. *Nature 402*, 778−784.
(16) Nitta, R., Kikkawa, M., Okada, Y., and Hirokawa, N. (2004) KIF1A alternately uses two loops to bind microtubules. *Science 305*, 678−683.
(17) Okada, Y., and Hirokawa, N. (1999) A processive single-headed motor: Kinesin superfamily protein KIF1A. *Science 283*, 1152−1157.
(18) Kikkawa, M., Sablin, E. P., Okada, Y., Yajima, H., Fletterick, R. J., and Hirokawa, N. (2001) Switch-based mechanism of kinesin motors. *Nature 411*, 439−445.
(19) Nitta, R., Okada, Y., and Hirokawa, N. (2008) Structural model for strain-dependent microtubule activation of Mg-ADP release from kinesin. *Nat. Struct. Mol. Biol. 15*, 1067−1075.
(20) Nogales, E., Wolf, S. G., and Downing, K. H. (1998) Structure of the $\alpha\beta$ tubulin dimer by electron crystallography. *Nature 391*, 199−203.
(21) Nogales, E., Whittaker, M., Milligan, R. A., and Downing, K. H. (1999) High-resolution model of the microtubule. *Cell 96*, 79−88.
(22) Sosa, H., Dias, D. P., Hoenger, A., Whittaker, M., Wilson-Kubalek, E., Sablin, E., Fletterick, R. J., Vale, R. D., and Milligan, R. A. (1997) A model for the microtubule-Ncd motor protein complex obtained by cryo-electron microscopy and image analysis. *Cell 90*, 217−224.
(23) Kozielski, F., Arnal, I., and Wade, R. H. (1998) A model of the microtubule-kinesin complex based on electron cryomicroscopy and X-ray crystallography. *Curr. Biol. 8*, 191−198.
(24) Hoenger, A., Sack, S., Thormahlen, M., Marx, A., Muller, J., Gross, H., and Mandelkow, E. (1998) Image reconstructions of microtubules decorated with monomeric and dimeric kinesins: Comparison with X-ray structure and implications for motility. *J. Cell Biol. 141*, 419−430.
(25) Hirose, K., Lowe, J., Alonso, M., Cross, R. A., and Amos, L. A. (1999) Congruent docking of dimeric kinesin and ncd into three-dimensional electron cryomicroscopy maps of microtubule-motor ADP complexes. *Mol. Biol. Cell 10*, 2063−2074.
(26) Kikkawa, M., Okada, Y., and Hirokawa, N. (2000) 15 Å resolution model of the monomeric kinesin motor, KIF1A. *Cell 100*, 241−252.
(27) Fisher, M. E., and Kolomeisky, A. B. (2001) Simple mechanochemistry describes the dynamics of kinesin molecules. *Proc. Natl. Acad. Sci. U.S.A. 98*, 7748−7753.
(28) Peskin, C. S., and Oster, G. (1995) Coordinated hydrolysis explains the mechanical behavior of kinesin. *Biophys. J. 68*, 202S−211S.
(29) Zheng, W., and Doniach, S. (2003) A comparative study of motor-protein motions by using a simple elastic-network model. *Proc. Natl. Acad. Sci. U.S.A. 100*, 13253−13258.
(30) Zheng, W., and Brooks, B. R. (2005) Normal-modes-based prediction of protein conformational changes guided by distance constraints. *Biophys. J. 88*, 3109−3117.
(31) Zheng, W., Brooks, B. R., and Hummer, G. (2007) Protein conformational transitions explored by mixed elastic network models. *Proteins 69*, 43−57.
(32) Zheng, W., and Tekpinar, M. (2009) Large-scale evaluation of dynamically important residues in proteins predicted by the perturbation analysis of a coarse-grained elastic model. *BMC Struct. Biol. 9*, 45.
(33) Hyeon, C., and Onuchic, J. N. (2007) Mechanical control of the directional stepping dynamics of the kinesin motor. *Proc. Natl. Acad. Sci. U.S.A. 104*, 17382−17387.
(34) Karplus, M., and McCammon, J. A. (2002) Molecular dynamics simulations of biomolecules. *Nat. Struct. Biol. 9*, 646−652.
(35) Mackerell, A. D. Jr. (2004) Empirical force fields for biological macromolecules: Overview and issues. *J. Comput. Chem. 25*, 1584−1604.
(36) Behnke-Parks, W. M., Vendome, J., Honig, B., Maliga, Z., Moores, C., and Rosenfeld, S. S. (2011) Loop L5 acts as a conformational latch in the mitotic kinesin Eg5. *J. Biol. Chem. 286*, 5242−5253.
(37) Zhang, W. (2011) Exploring the intermediate states of ADP-ATP exchange: A simulation study on Eg5. *J. Phys. Chem. B 115*, 784−795.
(38) Naber, N., Larson, A., Rice, S., Cooke, R., and Pate, E. (2011) Multiple conformations of the nucleotide site of Kinesin family motors in the triphosphate state. *J. Mol. Biol. 408*, 628−642.
(39) Hwang, W., Lang, M. J., and Karplus, M. (2008) Force generation in kinesin hinges on cover-neck bundle formation. *Structure 16*, 62−71.
(40) Aprodu, I., Soncini, M., and Redaelli, A. (2008) Interaction forces and interface properties of KIF1A kinesin-$\alpha\beta$ tubulin complex assessed by molecular dynamics. *J. Biomech. 41*, 3196−3201.
(41) Massova, I., and Kollman, P. A. (1999) Computational alanine scanning to probe protein-protein interactions: A novel approach to evaluate binding free energies. *J. Am. Chem. Soc. 121*, 8133−8143.
(42) Huo, S., Massova, I., and Kollman, P. A. (2002) Computational alanine scanning of the 1:1 human growth hormone-receptor complex. *J. Comput. Chem. 23*, 15−27.
(43) Moreira, I. S., Fernandes, P. A., and Ramos, M. J. (2006) Unraveling the importance of protein-protein interaction: Application of a computational alanine-scanning mutagenesis to the study of the IgG1 streptococcal protein G (C2 fragment) complex. *J. Phys. Chem. B 110*, 10962−10969.
(44) Cui, Q., Sulea, T., Schrag, J. D., Munger, C., Hung, M. N., Naim, M., Cygler, M., and Purisima, E. O. (2008) Molecular dynamics-solvated interaction energy studies of protein-protein interactions: The MP1-p14 scaffolding complex. *J. Mol. Biol. 379*, 787−802.
(45) Zoete, V., and Michielin, O. (2007) Comparison between computational alanine scanning and per-residue binding free energy decomposition for protein-protein association using MM-GBSA: Application to the TCR-p-MHC complex. *Proteins 67*, 1026−1047.
(46) Laitinen, T., Kankare, J. A., and Perakyla, M. (2004) Free energy simulations and MM-PBSA analyses on the affinity and specificity of steroid binding to antiestradiol antibody. *Proteins 55*, 34−43.
(47) Li, T., Froeyen, M., and Herdewijn, P. (2008) Computational alanine scanning and free energy decomposition for *E. coli* type I signal peptidase with lipopeptide inhibitor complex. *J. Mol. Graphics Modell. 26*, 813−823.
(48) Espinoza-Fonseca, L. M. (2009) Thermodynamic aspects of coupled binding and folding of an intrinsically disordered protein: A computational alanine scanning study. *Biochemistry 48*, 11332−11334.
(49) Hamza, A., Tong, M., AbdulHameed, M. D., Liu, J., Goren, A. C., Tai, H. H., and Zhan, C. G. (2010) Understanding microscopic binding of human microsomal prostaglandin E synthase-1 (mPGES-1) trimer with substrate PGH2 and cofactor GSH: Insights from computational alanine scanning and site-directed mutagenesis. *J. Phys. Chem. B 114*, 5605−5616.
(50) Zoete, V., and Meuwly, M. (2006) Importance of individual side chains for the stability of a protein fold: Computational alanine scanning of the insulin monomer. *J. Comput. Chem. 27*, 1843−1857.
(51) Hanes, M. S., Jude, K. M., Berger, J. M., Bonomo, R. A., and Handel, T. M. (2009) Structural and biochemical characterization of the interaction between KPC-2 β-lactamase and β-lactamase inhibitor protein. *Biochemistry 48*, 9185−9193.
(52) Sindelar, C. V., and Downing, K. H. (2007) The beginning of kinesin's force-generating cycle visualized at 9-Å resolution. *J. Cell Biol. 177*, 377−385.
(53) Kikkawa, M., and Hirokawa, N. (2006) High-resolution cryo-EM maps show the nucleotide binding pocket of KIF1A in open and closed conformations. *EMBO J. 25*, 4187−4194.
(54) Fiser, A., Do, R. K., and Sali, A. (2000) Modeling of loops in protein structures. *Protein Sci. 9*, 1753−1773.
(55) Humphrey, W., Dalke, A., and Schulten, K. (1996) VMD: Visual molecular dynamics. *J. Mol. Graphics 14*, 33−38.
(56) Martyna, G. J., Tobias, D. J., and Klein, M. L. (1994) Constant-Pressure Molecular-Dynamics Algorithms. *J. Chem. Phys. 101*, 4177−4189.

(57) Deserno, M., and Holm, C. (1998) How to mesh up Ewald sums. I. A theoretical and numerical comparison of various particle mesh routines. *J. Chem. Phys. 109*, 7678−7693.
(58) Hoover, W.G. (1985) Canonical Dynamics: Equilibrium Phase-Space Distributions. *Phys. Rev. A 31*, 1695−1697.
(59) Phillips, J.C., Braun, R., Wang, W., Gumbart, J., Tajkhorshid, E., Villa, E., Chipot, C., Skeel, R. D., Kale, L., and Schulten, K. (2005) Scalable molecular dynamics with NAMD. *J. Comput. Chem. 26*, 1781−1802.
(60) MacKerell, A. D., Bashford, D., Bellott, M., Dunbrack, R. L., Evanseck, J. D., Field, M. J., Fischer, S., Gao, J., Guo, H., Ha, S., Joseph-McCarthy, D., Kuchnir, L., Kuczera, K., Lau, F. T. K., Mattos, C., Michnick, S., Ngo, T., Nguyen, D. T., Prodhom, B., Reiher, W. E., Roux, B., Schlenkrich, M., Smith, J. C., Stote, R., Straub, J., Watanabe, M., Wiorkiewicz-Kuczera, J., Yin, D., and Karplus, M. (1998) All-atom empirical potential for molecular modeling and dynamics studies of proteins. *J. Phys. Chem. B 102*, 3586−3616.
(61) Foloppe, N., and MacKerell, A. D. (2000) All-atom empirical force field for nucleic acids: I. Parameter optimization based on small molecule and condensed phase macromolecular target data. *J. Comput. Chem. 21*, 86−104.
(62) Kollman, P. A., Massova, I., Reyes, C., Kuhn, B., Huo, S., Chong, L., Lee, M., Lee, T., Duan, Y., Wang, W., Donini, O., Cieplak, P., Srinivasan, J., Case, D. A., and Cheatham, T. E. III (2000) Calculating structures and free energies of complex molecules: Combining molecular mechanics and continuum models. *Acc. Chem. Res. 33*, 889−897.
(63) Nordman, N., Valjakka, J., and Perakyla, M. (2003) Analysis of the binding energies of testosterone, 5α-dihydrotestosterone, androstenedione and dehydroepiandrosterone sulfate with an antitestosterone antibody. *Proteins 50*, 135−143.
(64) Reyes, C. M., and Kollman, P. A. (2000) Structure and thermodynamics of RNA-protein binding: Using molecular dynamics and free energy analyses to calculate the free energies of binding and conformational change. *J. Mol. Biol. 297*, 1145−1158.
(65) Perakyla, M., and Nordman, N. (2001) Energetic analysis of binding of progesterone and 5β-androstane-3,17-dione to anti-progesterone antibody DB3 using molecular dynamics and free energy calculations. *Protein Eng. 14*, 753−758.
(66) Bradshaw, R. T., Patel, B. H., Tate, E. W., Leatherbarrow, R. J., and Gould, I. R. (2011) Comparing experimental and computational alanine scanning techniques for probing a prototypical protein-protein interaction. *Protein Eng., Des. Sel. 24*, 197−207.
(67) Moreira, I. S., Fernandes, P. A., and Ramos, M. J. (2007) Computational alanine scanning mutagenesis: An improved methodological approach. *J. Comput. Chem. 28*, 644−654.
(68) Lee, M. S., and Olson, M. A. (2006) Calculation of absolute protein-ligand binding affinity using path and endpoint approaches. *Biophys. J. 90*, 864−877.
(69) Eriksson, M. A. L., and Roux, B. (2002) Modeling the structure of Agitoxin in complex with the Shaker K^+ channel: A computational approach based on experimental distance restraints extracted from thermodynamic mutant cycles. *Biophys. J. 83*, 2595−2609.
(70) Gilson, M. K., and Honig, B. H. (1988) Energetics of Charge-Charge Interactions in Proteins. *Proteins 3*, 32−52.
(71) Im, W., Beglov, D., and Roux, B. (1998) Continuum Solvation Model: Computation of electrostatic forces from numerical solutions to the Poisson-Boltzmann equation. *Comput. Phys. Commun. 111*, 59−75.
(72) Dong, F., Vijayakumar, M., and Zhou, H. X. (2003) Comparison of calculation and experiment implicates significant electrostatic contributions to the binding stability of barnase and barstar. *Biophys. J. 85*, 49−60.
(73) Gorham, R. D., Kieslich, C. A., Nichols, A., Sausman, N. U., Foronda, M., and Morikis, D. (2011) An Evaluation of Poisson-Boltzmann Electrostatic Free Energy Calculations through Comparison with Experimental Mutagenesis Data. *Biopolymers*, h DOI: doi: 10.1002/bip.21644.
(74) Schutz, C. N., and Warshel, A. (2001) What are the dielectric "constants" of proteins and how to validate electrostatic models? *Proteins 44*, 400−417.
(75) Sham, Y. Y., Muegge, I., and Warshel, A. (1998) The effect of protein relaxation on charge-charge interactions and dielectric constants of proteins. *Biophys. J. 74*, 1744−1753.
(76) Olson, M. A., and Reinke, L. T. (2000) Modeling implicit reorganization in continuum descriptions of protein-protein interactions. *Proteins 38*, 115−119.
(77) Muegge, I., Schweins, T., and Warshel, A. (1998) Electrostatic contributions to protein-protein binding affinities: Application to Rap/Raf interaction. *Proteins 30*, 407−423.
(78) Gilson, M. K., and Honig, B. H. (1986) The dielectric constant of a folded protein. *Biopolymers 25*, 2097−2119.
(79) Sharp, K. A., and Honig, B. (1990) Electrostatic Interactions in Macromolecules: Theory and Applications. *Annu. Rev. Biophys. Biochem. 19*, 301−332.
(80) Sharp, K. A., and Honig, B. (1990) Calculating Total Electrostatic Energies with the Nonlinear Poisson-Boltzmann Equation. *J. Phys. Chem. 94*, 7684−7692.
(81) Harvey, S. C., and Hoekstra, P. (1972) Dielectric-Relaxation Spectra of Water Adsorbed on Lysozyme. *J. Phys. Chem. 76*, 2987.
(82) Roux, B. (1997) Influence of the membrane potential on the free energy of an intrinsic protein. *Biophys. J. 73*, 2980−2989.
(83) Nina, M., Beglov, D., and Roux, B. (1997) Atomic radii for continuum electrostatics calculations based on molecular dynamics free energy simulations. *J. Phys. Chem. B 101*, 5239−5248.
(84) Brooks, B. R., Bruccoleri, R. E., Olafson, B. D., States, D. J., Swaminathan, S., and Karplus, M. (1983) Charmm: A Program for Macromolecular Energy, Minimization, and Dynamics Calculations. *J. Comput. Chem. 4*, 187−217.
(85) Gohlke, H., Kiel, C., and Case, D. A. (2003) Insights into protein-protein binding by binding free energy calculation and free energy decomposition for the Ras-Raf and Ras-RaIGDS complexes. *J. Mol. Biol. 330*, 891−913.
(86) Almlof, M., Brandsdal, B. O., and Aqvist, J. (2004) Binding affinity prediction with different force fields: Examination of the linear interaction energy method. *J. Comput. Chem. 25*, 1242−1254.
(87) Ashkenazy, H., Erez, E., Martz, E., Pupko, T., and Ben-Tal, N. (2010) ConSurf 2010: Calculating evolutionary conservation in sequence and structure of proteins and nucleic acids. *Nucleic Acids Res. 38*, W529−W533.
(88) Landau, M., Mayrose, I., Rosenberg, Y., Glaser, F., Martz, E., Pupko, T., and Ben-Tal, N. (2005) ConSurf 2005: The projection of evolutionary conservation scores of residues on protein structures. *Nucleic Acids Res. 33*, W299−W302.
(89) Glaser, F., Pupko, T., Paz, I., Bell, R. E., Bechor-Shental, D., Martz, E., and Ben-Tal, N. (2003) ConSurf: Identification of Functional Regions in Proteins by Surface-Mapping of Phylogenetic Information. *Bioinformatics 19*, 163−164.
(90) Sheinerman, F. B., and Honig, B. (2002) On the role of electrostatic interactions in the design of protein-protein interfaces. *J. Mol. Biol. 318*, 161−177.
(91) Srinivasan, J., Miller, J., Kollman, P. A., and Case, D. A. (1998) Continuum solvent studies of the stability of RNA hairpin loops and helices. *J. Biomol. Struct. Dyn. 16*, 671−682.
(92) Aqvist, J., Medina, C., and Samuelsson, J. E. (1994) New Method for Predicting Binding-Affinity in Computer-Aided Drug Design. *Protein Eng. 7*, 385−391.
(93) Carlsson, J., Ander, M., Nervall, M., and Aqvist, J. (2006) Continuum solvation models in the linear interaction energy method. *J. Phys. Chem. B 110*, 12034−12041.
(94) Wall, I. D., Leach, A. R., Salt, D. W., Ford, M. G., and Essex, J. W. (1999) Binding constants of neuraminidase inhibitors: An investigation of the linear interaction energy method. *J. Med. Chem. 42*, 5142−5152.
(95) JonesHertzog, D. K., and Jorgensen, W. L. (1997) Binding affinities for sulfonamide inhibitors with human thrombin using Monte

Carlo simulations with a linear response method. *J. Med. Chem. 40*, 1539−1549.
(96) Lamb, M. L., Tirado-Rives, J., and Jorgensen, W. L. (1999) Estimation of the binding affinities of FKBP12 inhibitors using a linear response method. *Bioorg. Med. Chem. 7*, 851−860.
(97) Novotny, J., Bruccoleri, R. E., Davis, M., and Sharp, K. A. (1997) Empirical free energy calculations: A blind test and further improvements to the method. *J. Mol. Biol. 268*, 401−411.
(98) Wichapong, K., Lawson, M., Pianwanit, S., Kokpol, S., and Sippl, W. (2010) Postprocessing of Protein-Ligand Docking Poses Using Linear Response MM-PB/SA: Application to Wee1 Kinase Inhibitors. *J. Chem. Inf. Model. 50*, 1574−1588.
(99) Tidor, B., and Karplus, M. (1994) The Contribution of Vibrational Entropy to Molecular Association: The Dimerization of Insulin. *J. Mol. Biol. 238*, 405−414.
(100) Gohlke, H., and Case, D. A. (2004) Converging free energy estimates: MM-PB(GB)SA studies on the protein-protein complex Ras-Raf. *J. Comput. Chem. 25*, 238−250.
(101) Sharp, K. A. (1998) Calculation of HyHel10-Lysozyme binding free energy changes: Effect of ten point mutations. *Proteins 33*, 39−48.
(102) Norel, R., Sheinerman, F., Petrey, D., and Honig, B. (2001) Electrostatic contributions to protein-protein interactions: Fast energetic filters for docking and their physical basis. *Protein Sci. 10*, 2147−2161.
(103) Lee, L. P., and Tidor, B. (2001) Barstar is electrostatically optimized for tight binding to barnase. *Nat. Struct. Mol. Biol. 8*, 73−76.
(104) Barlow, D.J., and Thornton, J. M. (1983) Ion-Pairs in Proteins. *J. Mol. Biol. 168*, 867−885.
(105) Naber, N., Minehardt, T. J., Rice, S., Chen, X. R., Grammer, J., Matuska, M., Vale, R. D., Kollman, P. A., Car, R., Yount, R. G., Cooke, R., and Pate, E. (2003) Closing of the nucleotide pocket of kinesin-family motors upon binding to microtubules. *Science 300*, 798−801.
(106) Yun, M. Y., Zhang, X. H., Park, C. G., Park, H. W., and Endow, S. A. (2001) A structural pathway for activation of the kinesin motor ATPase. *EMBO J. 20*, 2611−2618.
(107) Okada, Y., and Hirokawa, N. (2000) Mechanism of the single-headed processivity: Diffusional anchoring between the K-loop of kinesin and the C terminus of tubulin. *Proc. Natl. Acad. Sci. U.S.A. 97*, 640−645.
(108) Klumpp, L. M., Hoenger, A., and Gilbert, S. P. (2004) Kinesin's second step. *Proc. Natl. Acad. Sci. U.S.A. 101*, 3444−3449.
(109) Rice, S., Lin, A. W., Safer, D., Hart, C. L., Naber, N., Carragher, B. O., Cain, S. M., Pechatnikova, E., Wilson-Kubalek, E. M., Whittaker, M., Pate, E., Cooke, R., Taylor, E. W., Milligan, R. A., and Vale, R. D. (1999) A structural change in the kinesin motor protein that drives motility. *Nature 402*, 778−784.
(110) Auerbach, S. D., and Johnson, K. A. (2005) Kinetic effects of kinesin switch I and switch II mutations. *J. Biol. Chem. 280*, 37061−37068.
(111) Shimizu, T., Thorn, K. S., Ruby, A., and Vale, R. D. (2000) ATPase kinetic characterization and single molecule behavior of mutant human kinesin motors defective in microtubule-based motility. *Biochemistry 39*, 5265−5273.
(112) Klumpp, L. M., Hoenger, A., and Gilbert, S. P. (2004) Kinesin's second step. *Proc. Natl. Acad. Sci. U.S.A. 101*, 3444−3449.